Catalysis Science & Technology

PAPER

Cite this: *Catal. Sci. Technol.*, 2016, **6**, 8024

Ruthenium molecular complexes immobilized on graphene as active catalysts for the synthesis of carboxylic acids from alcohol dehydrogenation†‡

David Ventura-Espinosa,[a] Cristian Vicent,[b] Miguel Baya[c] and Jose A. Mata*[a]

Received 7th July 2016,
Accepted 26th September 2016

DOI: 10.1039/c6cy01455k

www.rsc.org/catalysis

Ruthenium complexes containing N-heterocyclic carbene ligands functionalized with different polyaromatic groups (pentafluorophenyl, anthracene, and pyrene) are immobilized onto the surface of reduced graphene oxide. The hybrid materials composed of organometallic complexes and graphene are obtained in a single-step process. The hybrid materials are efficient catalysts for the synthesis of carboxylic acids from the dehydrogenation of alcohols in aqueous media. The catalytic materials can be recycled up to ten times without significant loss of activity. The catalytic activity of the pyrene derivative, Pyr–Ru (**3**) is enhanced when the ruthenium complex is anchored onto the surface of graphene. The carbonaceous material limits the degradation of the ruthenium complex resulting in increased activity and requiring lower catalyst loading. The catalytic process of the pyrene hybrid material is heterogeneous in nature due to the strong interaction between the pyrene and graphene. The catalytic process of the anthracene and pentafluorophenyl hybrid materials is governed by the so-called 'boomerang effect'. The ruthenium molecular complex is released from and returned to the graphene surface during the catalytic reaction. Mechanistic insight has been obtained experimentally and theoretically. The energy profile suggests that the rate-determining step is the nucleophilic attack of water on a coordinated aldehyde complex to form a *gem*-diolate complex.

Introduction

The growing interest in molecular complexes immobilized on the surface of graphene has arisen due to the possibility they offer of combining the advantages of both homogeneous and heterogeneous catalysis.[1–3] Well-defined molecular complexes can be finely tuned by ligand modification to achieve highly desired properties.[4,5] Ligands can confer high activity and stability to the catalyst by modifying the electronic and steric properties of the metal centre and, in particular, increasing its selectivity.[6–8] Graphene is a convenient support for catalytic applications due to its high surface area.[9–12] The 2D structure of graphene enables complete accessibility to all catalytically active centres. This is an important factor in order to increase the catalytic activity by avoiding diffusion problems. The immobilization of molecular complexes onto solid surfaces facilitates the separation of the catalysts from the reaction media by simple filtration, which can then be reused in multiple subsequent cycles. Ideally, a support should also increase the catalytic activity by avoiding possible decomposition pathways. The immobilization process should involve the formation of a strong linkage between graphene and the molecular complex in order to afford better performances in terms of recovery and reuse. Graphene contains a delocalized π-electronic system that allows immobilization of polyaromatic rings by π-stacking interactions.[13–15] We have previously developed a methodology that does not require the functionalization of graphene, and by which different metal complexes containing a pyrene fragment were anchored onto the surface of reduced graphene oxide (rGO) by means of π-stacking interactions.[16–18] The results revealed that the complexes were strongly adsorbed onto the graphene surface. This immobilization process is straightforward, minimizing costs and reaction steps, and thus possesses great potential for industrial applications.[19,20]

The oxidation of alcohols is an interesting transformation for the synthesis of carboxylic acids and related species.[21–25] Catalytic procedures employing oxygen or hydrogen peroxide

[a] *Institute of Advanced Materials (INAM), Universitat Jaume I, Avda. Sos Baynat s/n, 12006, Castellón, Spain. E-mail: jmata@uji.es; Fax: +34 964387522; Tel: +34 964387516*
[b] *Serveis Centrals d'Intrumentació Científica (SCIC), Universitat Jaume I, Avda. Sos Baynat s/n, 12071, Castellón, Spain*
[c] *Instituto de Síntesis Química y Catálisis Homogénea (ISQCH), Departamento de Química Inorgánica, CSIC-Universidad de Zaragoza, C/Pedro Cerbuna 12, E-50009 Zaragoza, Spain*

† The authors declare no competing financial interest.

‡ Electronic supplementary information (ESI) available. CCDC 1489562 and 1489563. For ESI and crystallographic data in CIF or other electronic format see DOI: 10.1039/c6cy01455k

as an oxidant represent an improvement over traditional stoichiometric methodologies.[26] Milstein *et al.* have recently described the synthesis of carboxylic acids from the dehydrogenation of alcohols using water as the terminal oxidant.[27] The process is very attractive due to the one-step synthesis of carboxylic acids, the use of a non-toxic oxidant and the formation of valuable molecular hydrogen. The literature on the direct catalytic synthesis of carboxylic acids from alcohols is scarce and few reports have been described for ruthenium,[27–30] palladium,[31] and rhodium.[32] Alcohol dehydrogenation is especially relevant in the case of methanol as, under basic aqueous conditions, it generates three moles of hydrogen gas and carbon dioxide. Methanol is a good hydrogen carrier with a high hydrogen capacity and can be produced from renewable resources. Thus, this organic compound is considered as a promising alternative to traditional fossil fuel energy.[33–36]

In this work, we describe the immobilization on graphene of new ruthenium complexes with different polyaromatic groups. The introduction of various functional groups as linkers allows the evaluation of the non-covalent interactions between graphene and the molecular ruthenium complexes. We have evaluated the catalytic properties of the hybrid materials in the dehydrogenation of alcohols to produce carboxylic acids in aqueous media. Graphene has a positive effect on the catalysts, resulting in higher activity and stability. The supported catalytic reaction displays a distinct operating mechanism depending on the polyaromatic group used to anchor the molecular complex onto graphene. The mechanism of the catalytic dehydrogenation of alcohols has been studied at the molecular level under homogeneous conditions. A plausible mechanism is proposed based on experimental evidence and theoretical calculations. This work demonstrates the advantages of supported molecular catalysis and offers a practical methodology, which may inspire future developments toward efficient heterogeneous catalysts.

Results and discussion

Synthesis of ruthenium complexes and hybrid materials

The imidazolium salts PhF,[37] Ant,[38] and Pyr,[16] functionalized with aromatic systems, were obtained according to reported procedures. The synthesis comprises the alkylation of methylimidazole with the corresponding chloro or bromomethyl arene (Scheme 1). Reaction of the imidazolium salts with silver oxide affords silver carbene complexes that are then used as carbene transfer reagents. On reaction with $[Ru(p\text{-cym})Cl_2]_2$, the ruthenium complexes PhF–Ru (**1**) and Ant–Ru (**2**) are obtained. The synthesis and properties of complex **3** and the hybrid material **6** have been previously described.[16] Complexes PhF–Ru (**1**) and Ant–Ru (**2**) were characterized by NMR spectroscopy, ESI-MS spectrometry, and elemental analysis. The ^{1}H NMR spectra confirmed the disappearance of the acidic signal of the imidazolium salt at high frequencies and the $^{13}C\{^1H\}$ NMR spectra showed the characteristic signal for $M–C_{carbene}$ at 175.9 ppm for PhF–Ru (**1**) and 172.6 ppm for Ant–Ru (**2**). Positive ion ESI mass spectrum analysis (ESI-MS) in MeCN of complexes PhF–Ru (**1**) and Ant–Ru (**2**) showed a base peak for $[M - X]^+$ at m/z = 533.0 and m/z = 543.1, respectively, which confirms the proposed molecular composition of the complexes based on the mass/charge relation and the isotopic pattern. Metal–halide bond-breaking is a common and well-documented ionization mechanism under ESI conditions for a wide range of neutral halide complexes.[39,40]

The molecular structure of compounds PhF–Ru (**1**) and Pyr–Ru (**3**) was further confirmed by means of X-ray diffraction. The structure analysis reveals a ruthenium centre with a *p*-cymene moiety, two chlorides and the NHC ligand in a piano-stool coordination environment (Fig. 1 and 2). According to the bond lengths and angles, the geometry around the two ruthenium centres is similar; for instance, the $Ru–C_{carbene}$ distance is 2.065(3) Å for compound PhF–Ru (**1**) and 2.081(3) Å for compound Pyr–Ru (**3**). More interesting is the arrangement in the crystal. The packing diagram of complex Pyr–Ru (**3**) shows an intermolecular slipped π-stacking between pairs of molecules with an interplanar distance of 3.61 Å (Fig. 2). This π–π interaction has also been observed in a palladium complex bearing an NHC ligand functionalized with a pyrene fragment.[16] The π-stacking between pairs of molecules is an indication of the predisposition of the pyrene moiety to display this type of interactions.[41] This stacking is not observed in the case of compound PhF–Ru (**1**), functionalized with a pentafluorobenzyl group. Most likely, the NHC-pentafluorobenzyl

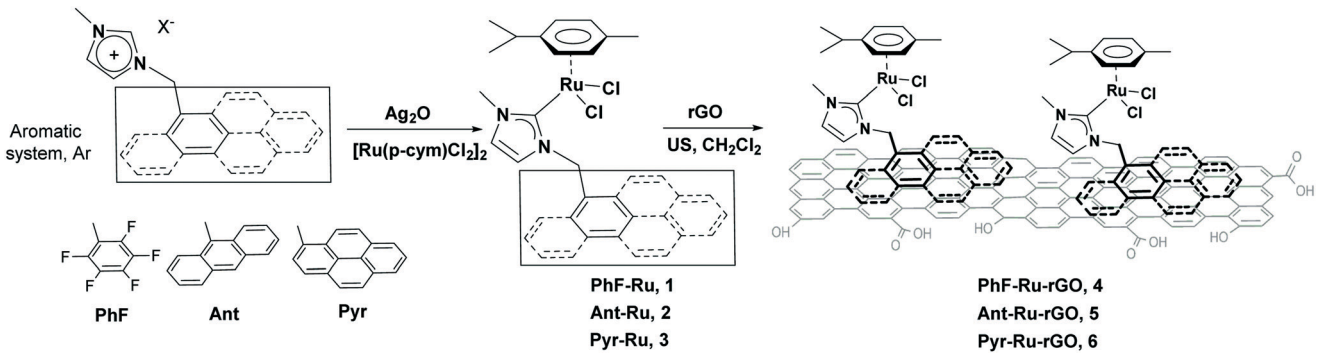

Scheme 1

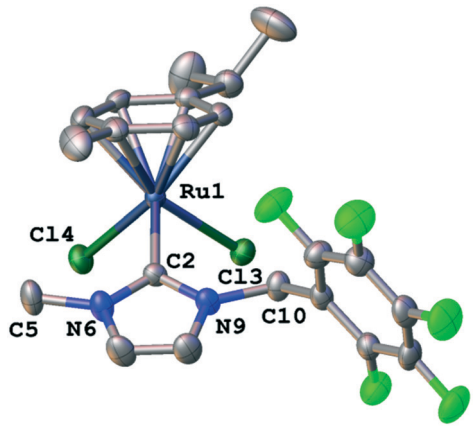

Fig. 1 Molecular diagram of compound PhF–Ru, **1**. Ellipsoids are at 50% probability level. Hydrogen atoms and crystallization solvent (chloroform) have been omitted for clarity. Selected bond lengths [Å] and angles [°]: Ru(1)–C(2) 2.065(3), Ru(1)–Cl(3) 2.4229(7), Ru(1)–Cl(4) 2.4205(7), Ru(1)–Ph_{cent} 1.69, C(2)–N(6) 1.360(3), C(2)–N(9) 1.365(3), Cl(3)–Ru(1)–Cl(4) 84.65(2), C(2)–Ru(1)–Cl(3) 89.81(8), C(2)–Ru(1)–Cl(4) 90.05(7), N(6)–C(2)–N(9) 103.3(2).

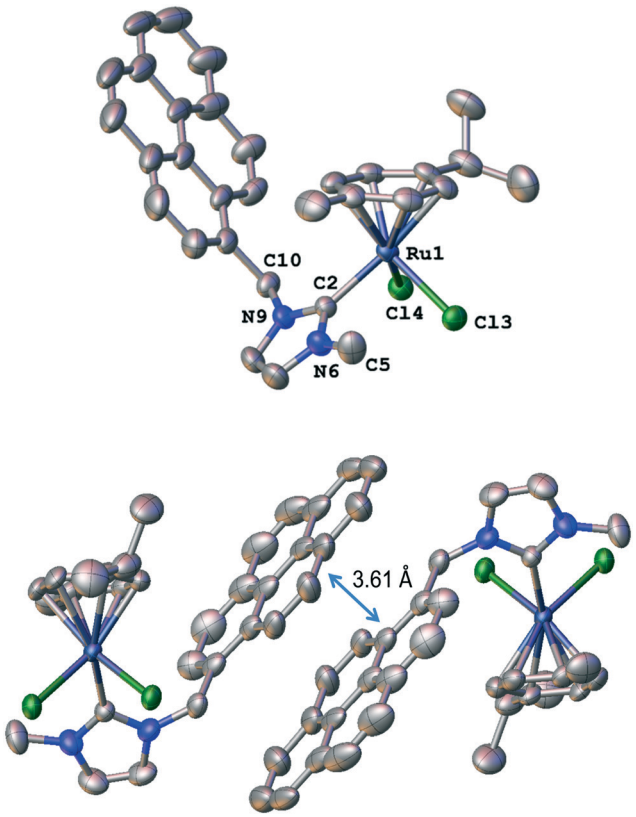

Fig. 2 Molecular diagram (top) and crystal packing (bottom) of compound Pyr–Ru, **3**. Ellipsoids are at 50% probability level. Hydrogen atoms and crystallization solvents (chloroform and *n*-hexane) have been omitted for clarity. Selected bond lengths [Å] and angles [°]: Ru(1)–C(2) 2.081(3), Ru(1)–Cl(3) 2.4282(10), Ru(1)–Cl(4) 2.4312(9), Ru(1)–Ph_{cent} 1.684, C(2)–N(6) 1.354(5), C(2)–N(9) 1.360(5), Cl(3)–Ru(1)–Cl(4) 84.16(3), C(2)–Ru(1)–Cl(3) 91.02(10), C(2)–Ru(1)–Cl(4) 88.03(10), N(6)–C(2)–N(9) 104.1(3). The π-stacking interplanar distance is 3.61 Å.

ligand has a major tendency to form hydrogen-bonds rather than π-stacked structures.

The hybrid organometallic-graphene materials **4–6** were obtained using a methodology previously reported.[16] The molecular ruthenium complexes **1–3** were mixed with reduced graphene oxide (rGO) in dichloromethane in an ultrasound bath for 30 min, followed by stirring for 10 h. The first evidence for the anchoring of the molecular complex Pyr–Ru (**3**) onto the surface of rGO was provided by the disappearance of the colour of the reaction solution. The yellow colour of the dichloromethane solution with complex Pyr–Ru (**3**) gradually disappeared as the complex was being adsorbed onto the surface of rGO. In the case of complexes PhF–Ru (**1**) and Ant–Ru (**2**), the colour of the solution did not disappear completely, indicating that not all the molecular complex had been anchored on the surface of the material. The exact ruthenium content on the hybrid materials **4–6** was determined by digestion of the samples in hot HCl/HNO_3 followed by ICP-MS analysis. The ruthenium content anchored on rGO would have been 10 wt% if all the molecular complex had been retained on the support. The results obtained by ICP-MS analysis accounted for 1.0 wt% of **1** in PhF–Ru–rGO (**4**), 3.2 wt% of **2** in Ant–Ru–rGO (**5**), and 9.1 wt% of **3** in Pyr–Ru–rGO (**6**). As expected, the molecular complex containing the pentafluorobenzyl group (**1**) is barely retained on the surface of rGO. In contrast, the ruthenium complex containing the pyrene fragment (**3**) is retained almost quantitatively. These results correlate with the proclivity of the different aromatic rings to form π-stacking interactions,[42] as an increasing number of aromatic rings increases the strength of π–π interactions.[43] The ruthenium complex **3**, containing a pyrene aromatic group with four rings, is anchored more efficiently on the surface of rGO. These results were further supported by single crystal X-ray diffraction. Complex PhF–Ru (**1**) does not display a clear tendency to form π-stacking interactions and, as a consequence, it is barely retained on the surface of rGO. Complex Pyr–Ru (**3**), containing a pyrene tag, shows a clear tendency to form dimers by π-stacking interactions, and the results show that it is strongly anchored onto rGO. The immobilization of complex Ant–Ru (**2**), containing an anthracene moiety, corresponds to an intermediate situation. We have previously observed that a ruthenium complex without any aromatic group $[RuCl_2(I_{n\text{-Bu}})(p\text{-cymene})]_2$ ($I_{n\text{-Bu}}$ = 1,3-di-*n*-butylimidazolylidene) is not retained on rGO under the same reaction conditions. The results suggest that the presence of aromatic groups is necessary for immobilization on the surface of graphene and that, most probably, the operating driving force is π-stacking.[41] The characterization of the hybrid materials **4–6** was performed using UV/vis, FTIR, and Raman spectroscopy, SEM, and HRTEM (see the ESI‡ for details). Elemental mapping by energy-dispersive X-ray spectroscopic analysis (EDS) performed by means of HRTEM of PhF–Ru–rGO (**4**) and Ant–Ru–rGO (**5**) confirmed the homogeneous distribution of ruthenium in these two hybrid materials (Fig. 3), as it has also been observed previously in the case of the Pyr–Ru–rGO (**6**) material.

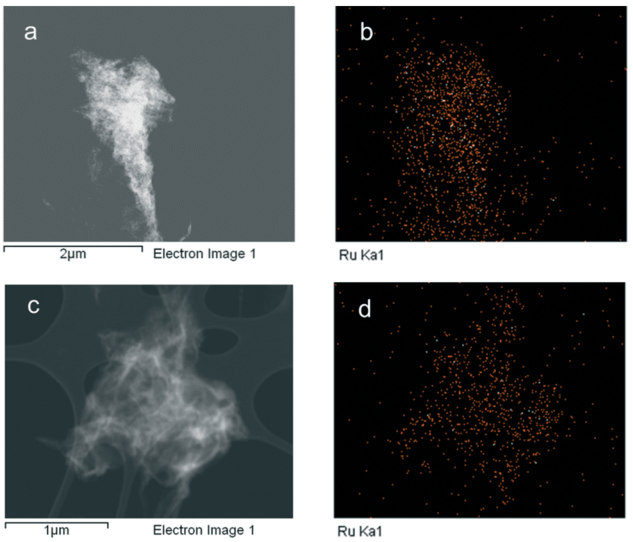

Fig. 3 STEM images (left) and EDS elemental mapping (right) images showing the homogeneous distribution of ruthenium on the hybrid materials PhF–Ru–rGO (**4**) (a and b) and Ant–Ru–rGO (**5**) (c and d).

Catalytic applications

The catalytic properties of the ruthenium hybrid materials were tested in the acceptorless dehydrogenation of alcohols to carboxylic acids in aqueous media. In a first set of experiments, the catalytic activity of the ruthenium molecular complexes and the hybrid materials was studied using benzyl alcohol as the model substrate (Table 1). A blank experiment using only rGO revealed that the support is not active in the dehydrogenation of alcohols (Table 1, entry 1). In recent years, the use of chemically-derived graphene materials as efficient carbocatalysts has been described. In general, carbocatalytic systems require high catalyst loadings and numerous oxygen-containing functionalities. The quantity of rGO used in our experiments is low and the catalytic activity of the support is negligible.[44–47] The molecular ruthenium complexes and the corresponding hybrid materials are active in the dehydrogenation of benzyl alcohol with high selectivity towards the carboxylate. We did not observe the formation of by-products such as esters or hemiacetals. The dehydrogenation of benzyl alcohol using the hybrid materials **4**–**6** at a catalyst loading (based on ruthenium) of 0.1 mol% afforded moderate to good conversions (Table 1, entries 3, 6 and 9). When the catalyst loading was increased to 1 mol%, quantitative conversions of benzyl alcohol were observed (Table 1, entries 4, 7 and 10). Isolation of pure benzoic acid was obtained after acidification. The dehydrogenation of benzyl alcohol using the molecular complex Pyr–Ru (**3**) at a catalyst loading of 0.1 mol% afforded low conversion, 11% (Table 1, entry 8). On the contrary, when the dehydrogenation of benzyl alcohol is carried out using the hybrid material Pyr–Ru–rGO (**6**), under the same reaction conditions, the conversion increased to 74% (Table 1, entry 9). This result suggests that although the molecular catalyst is active in the formation of carboxylic acids there is a competing deactivation process. The nature of the deactivation process is unknown but it is suppressed when the molecular complex is anchored on graphene. The immobilization of the molecular catalysts onto rGO provides a catalytic benefit caused by stabilisation of the catalytically active species. We have previously observed the same tendency in the catalytic formation of benzaldehyde from the dehydrogenation of benzyl alcohol using toluene as solvent.[16]

The ruthenium hybrid materials **4**–**6** were tested in the dehydrogenation of a series of substrates. The results obtained for different substituted benzyl alcohols are shown in Table 2. The three hybrid materials are active in the dehydrogenation of different benzyl alcohols in water, affording good to full conversions at low catalyst loadings. All the products were isolated and identified by means of ^{1}H NMR spectroscopy after acidification. The best result was obtained for the dehydrogenation of (*p*-trifluoromethyl)benzyl alcohol with

Table 1 Catalyst screening: acceptorless dehydrogenation of benzyl alcohol to benzoic acid

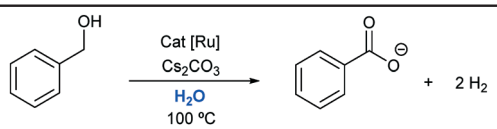

Entry	Catalyst	[Ru] mol%	Conversion[a] (%)
1	rGO	—	0
2	PhF–Ru (**1**)	0.2	43
3	PhF–Ru–rGO (**4**)	0.1	65
4	PhF–Ru–rGO (**4**)	1	98 (87)
5	Ant–Ru (**2**)	2	44
6	Ant–Ru–rGO (**5**)	0.1	89 (76)
7	Ant–Ru–rGO (**5**)	1	100 (95)
8	Pyr–Ru (**3**)	0.1	11
9	Pyr–Ru–rGO (**6**)	0.1	74 (70)
10	Pyr–Ru–rGO (**6**)	1	100 (93)

Reaction conditions: benzyl alcohol (0.5 mmol), Cs_2CO_3 (1 eq.), catalyst, 10 mL of water at 100 °C for 24 h. [a] Conversion determined by GC analysis using anisole as the standard. Isolated yield after acidification in parenthesis determined by ^{1}H NMR using trimethoxybenzene as the standard.

Table 2 Dehydrogenation of substituted benzylic alcohols in water

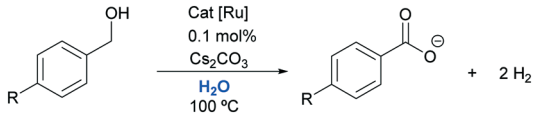

Entry	Catalyst	R	Conversion[a] (%)
1	PhF–Ru–rGO (**4**)	Me	90 (85)
2	PhF–Ru–rGO (**4**)	Cl	75
3	PhF–Ru–rGO (**4**)	Br	85
4	PhF–Ru–rGO (**4**)	CF_3	89
5	Ant–Ru–rGO (**5**)	Me	88
6	Ant–Ru–rGO (**5**)	Cl	82 (80)
7	Ant–Ru–rGO (**5**)	Br	99 (90)
8	Ant–Ru–rGO (**5**)	CF_3	100 (92)
9	Pyr–Ru–rGO (**6**)	Me	76
10	Pyr–Ru–rGO (**6**)	Cl	73
11	Pyr–Ru–rGO (**6**)	Br	88
12	Pyr–Ru–rGO (**6**)	CF_3	97 (93)

Reaction conditions: substrate (0.5 mmol), Cs_2CO_3 (1 eq.), catalyst (0.1 mol %), 10 mL of water at 100 °C for 24 h. [a] Conversions determined by GC analysis using anisole as the standard. Isolated yield after acidification in parenthesis determined by ^{1}H NMR using trimethoxybenzene as the standard.

catalyst Ant–Ru–rGO (**5**), which affords a quantitative conversion after 24 h (Table 2, entry 8). The time–conversion profile for this experiment is shown in Fig. S12.‡ In general, better results were obtained in the case of substrates with *p*-substituted electron-withdrawing groups.§

Recycling studies

In view of the good results obtained with the hybrid materials in the dehydrogenation of different benzyl alcohols, we decided to evaluate the stability of the catalysts and to explore their recyclability. Recycling experiments were carried out using (*p*-trifluoromethyl)benzyl alcohol as the model substrate. The reactions were performed using the conditions described previously and the reaction progress was monitored by GC. After 12 h of reaction (*ca.* 50% conversion), the mixture was allowed to cool down to room temperature, and the solid catalyst was separated by decantation, washed thoroughly with water, and used again in another run (Fig. 4).

The three hybrid materials (**4–6**) were reused several times without any significant decrease in activity. These results are excellent, especially if we consider the low catalyst loadings used in the recycling experiments (0.1 mol%). The catalyst stability and recyclability depend on the tag used to anchor the molecular complex onto the surface of graphene. Catalyst PhF–Ru–rGO (**4**) was reused up to five times without any significant decrease in activity (from 48% in run 1 to 47% in run 5) and, in the seventh run, the conversion dropped to 40%. The ruthenium content in the solution of each run was analysed by ICP-MS. The results show that the ruthenium content in the solutions corresponding to runs 1–5 is negligible (less than 0.1 ppb). In contrast, the ruthenium content in solution for runs 6 and 7 accounts for 4 and 5 ppm, respectively. These results suggest that deactivation of the hybrid material PhF–Ru–rGO (**4**) is caused by leaching of the molecular complex from the surface of graphene. Catalyst Ant–Ru–rGO (**5**) was reused up to eight times without any significant decrease in activity and, in the tenth run, the conversion dropped to 40%. The ICP-MS analysis shows that the ruthenium loss by leaching is negligible until the eighth run. This hybrid material containing an anthracene group could be recycled more efficiently than catalyst **4**, containing a pentafluorinated phenyl ring. The best material in terms of

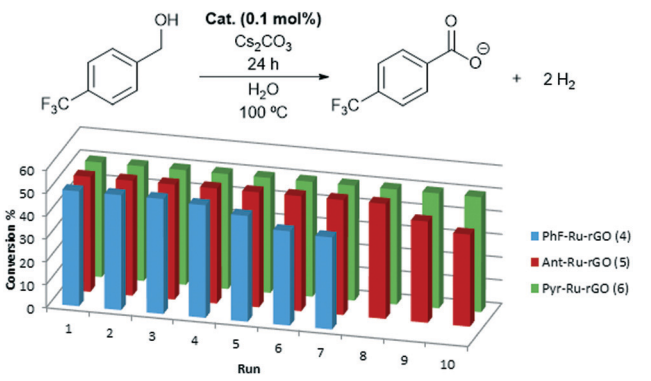

Fig. 4 Recycling experiments on the dehydrogenation of (*p*-trifluoromethyl)benzyl alcohol using hybrid materials **4–6**. Conversions determined by GC analysis after 12 h of reaction.

§ The ruthenium complexes **1–3** and the ruthenium hybrid materials **4–6** were tested in the dehydrogenation of aliphatic alcohols such as 2-phenylethanol and 1-hexanol. The reaction monitoring by GC show that full conversions are obtained under the reaction conditions described in Table 2. However, we have observed discrepancies between the conversion and the isolated yield after acidification and the results are not included in the manuscript. For instance, in the case of 1-hexanol, full conversion is observed in 24 h reaction but only 38% yield of 1-hexanoic acid was obtained after isolation. We have not included these preliminary results in the activation of aliphatic alcohols. Future work is in progress in our laboratory.

recyclability is the system with the pyrene tag. Catalyst Pyr–Ru–rGO (**6**) was reused up to ten times without any significant decrease in activity. The ICP-MS analysis shows that the amount of ruthenium in solution in the tenth run is negligible. The presence of a pyrene group favours the immobilization of the molecular complex onto the surface of graphene and, therefore, the stability of the catalyst improves.

The catalytic graphene materials were analysed after the recycling experiments by HRTEM in order to explore any possible changes in the material and/or the formation of metal nanoparticles. A comparison of the HRTEM images of the hybrid material PhF–Ru–rGO (**4**) before and after the recycling experiments reveals the same well-dispersed ruthenium distribution (Fig. 5). The EDS elemental mapping shows that there is no aggregation of ruthenium on graphene or formation of nanoparticles. Apparently, there is no modification of the support morphology and the material preserves its single layer nature. Similar analyses were performed for the hybrid materials Ant–Ru–rGO (**5**) and Pyr–Ru–rGO (**6**). The results show a good distribution of ruthenium all over the material surface without the formation of nanoparticles and changes in the morphology of graphene.

Non-covalent interactions between pyrene and carbon nanotubes have been reported for the immobilization of organometallic complexes.[48–51] A study on the catalytic properties of a gold complex with a pyrene-tag on carbon nanotubes proved that π–π stacking interactions are affected by solvent polarity and temperature. In fact, the release-and-return (boomerang effect) of this molecular complex from and to the support was observed, implying a homogeneous catalytic process.[52] In the case of non-covalent interactions between pyrene and reduced graphene oxide, we have previously observed that palladium and ruthenium complexes are strongly immobilized on the surface of rGO. In those catalytic experiments, we did not observe desorption of the molecular complexes in solvents such as dichloromethane, acetone, toluene, or isopropanol or by increasing the temperature.[16]

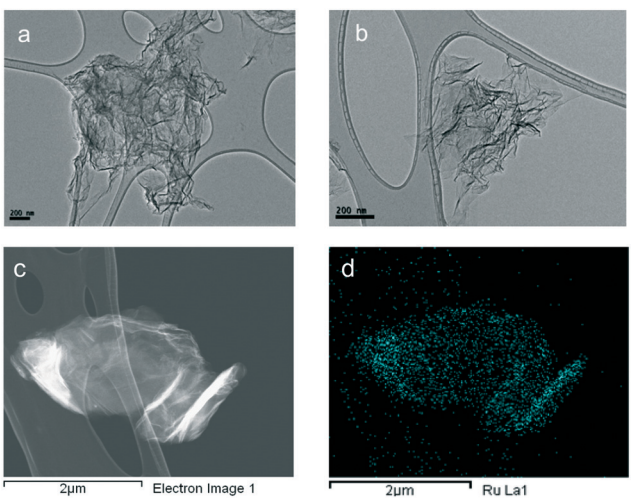

Fig. 5 HRTEM images of PhF–Ru–rGO (**4**) before (a) and after (b) seven catalytic runs. STEM (c) and EDS elemental mapping (d) images showing the homogeneous distribution of ruthenium after the seventh run.

In order to establish the possibility of release-and-return of the molecular complex from the surface of graphene, hot filtration experiments were carried out.[52–57] This type of experiment is used to distinguish between homogeneous and heterogeneous catalytic processes, especially in the case of supported molecular catalysts. In a first experiment, we used the pyrene containing hybrid material Pyr–Ru–rGO (**6**) and (*p*-trifluoromethyl) benzyl alcohol. After 12 h of reaction (GC conversion, 45%), the catalytic hybrid material (**6**) was removed by filtration at 100 °C. The filtrate was stirred for 12 h more under identical conditions. After this time, GC analysis indicated that no further alcohol oxidation had occurred (GC conversion remained at 45%). In a parallel experiment, the precipitate was treated with the substrate, solvent, and base. After 12 h of reaction, a conversion of 42% was observed, indicating the heterogeneous nature of the catalytic hybrid material **6**. The hot filtration experiment confirmed the absence of catalytic species in solution due to catalyst desorption from the graphene surface.

In the case of hybrid materials PhF–Ru–rGO (**4**) and Ant–Ru–rGO (**5**), the results were completely different. In the hot filtration experiments using (*p*-trifluoromethyl) benzyl alcohol as the model substrate, we observed that the catalytic reaction continued in the solution after filtration at 100 °C. In both cases, the hot filtration experiments confirmed that the molecular complexes had been released from the surface of graphene at high temperatures in aqueous media. The recycling properties indicate that, after the catalytic reaction, the molecular complexes are re-immobilized on the surface of graphene at low temperatures, allowing their reuse. Considering the boomerang effect, the catalytic properties of the molecular complexes and the related materials should be similar but according to the results of Table 1 (compare entries 2–3 and 5–6) the efficiency of the catalysts is different. A plausible explanation for the difference in catalyst activity is the effect produced by the rGO material. We believe that rGO increases the stability of the molecular complex and as a consequence increases the efficiency of the catalyst by trapping and releasing the molecular complex. Thus, a boomerang effect takes place and the catalytic process is homogeneous in nature, since the catalytic reaction happens in solution.

The hot filtration experiments demonstrate that hybrid materials PhF–Ru–rGO (**4**) and Ant–Ru–rGO (**5**) form weak π-stacking interactions with graphene. At high temperatures, the molecular complexes are released from the support. The mechanism that governs the catalytic properties is based on a boomerang effect. The hybrid material Pyr–Ru–rGO (**6**) containing a molecular complex with a pyrene-tag is strongly retained on the surface of graphene. No desorption was observed by changing the solvent or increasing the temperature. The hot filtration test revealed that the catalysis is heterogeneous in nature, indicating that the molecular complex is retained on the surface of graphene. The catalytic properties

are increased upon immobilization compared to those of the molecular complex most probably due to a stabilization of the catalytically active species. The presence of a pyrene group facilitates the immobilization of the molecular complex on the surface of graphene by π-stacking, compared to the pentafluorobenzyl or anthracene groups.

Mechanism

A plausible mechanism for the transformation of benzyl alcohol to carboxylate by the Ru–NHC complex is shown in Scheme 2. The proposal of the mechanism is based on experimental evidence obtained by NMR spectroscopy and electrospray ionization mass spectrometry (ESI-MS) and theoretical evidence obtained by DFT calculations.

The ruthenium complex **I** bearing an NHC ligand, *p*-cymene, and two chlorides is soluble in water. The observation of different species in solution agrees with the results described previously for a Ru complex featuring 1-butyl-3-methylimidazol-2-ylidene.[58] Complex PhF–Ru (**1**) was chosen as a representative member of the series of efficient catalysts investigated herein, and we addressed its chemical speciation both in aqueous solution and under catalytic conditions by NMR spectroscopy and ESI-MS. The ^{1}H NMR spectrum of an aqueous solution of PhF–Ru (**1**) displays signals for *p*-cymene and the NHC ligand which are consistent with those recorded in $CDCl_3$ (Fig. S13‡). Significant line broadening at room temperature and variable temperature behaviour are indicative of the co-existence of several species in equilibrium. All these species could not be unambiguously identified based on the ^{1}H and $^{13}C\{^{1}H\}$ NMR spectra. Detailed insight into the aqueous chemical speciation of PhF–Ru (**1**) was gathered from single-stage ESI-MS (see the ESI‡ for details). The ESI-MS results suggest that: i) immediate Ru–Cl cleavage and subsequent water coordination at the vacant site takes place rapidly upon dissolving PhF–Ru (**1**) in water, and ii) as the pH increases, the successive deprotonation of water molecules takes place (Scheme 3).

We next explored the ESI-MS data in the presence of benzyl alcohol under catalytic conditions. The ESI-MS spectra displayed species corresponding to the Ru-alkoxide and Ru-carboxylate species derived from the benzyl alcohol as well as signals attributed to hydride species, which is fully consistent with the occurrence of alcohol activation and dehydrogenation. A ruthenium-hydroxo based mechanism for alcohol activation under aqueous conditions has recently been described proposing a bifunctional catalysed process.[59] The reaction of benzyl alcohol with **I** under basic conditions yields the active

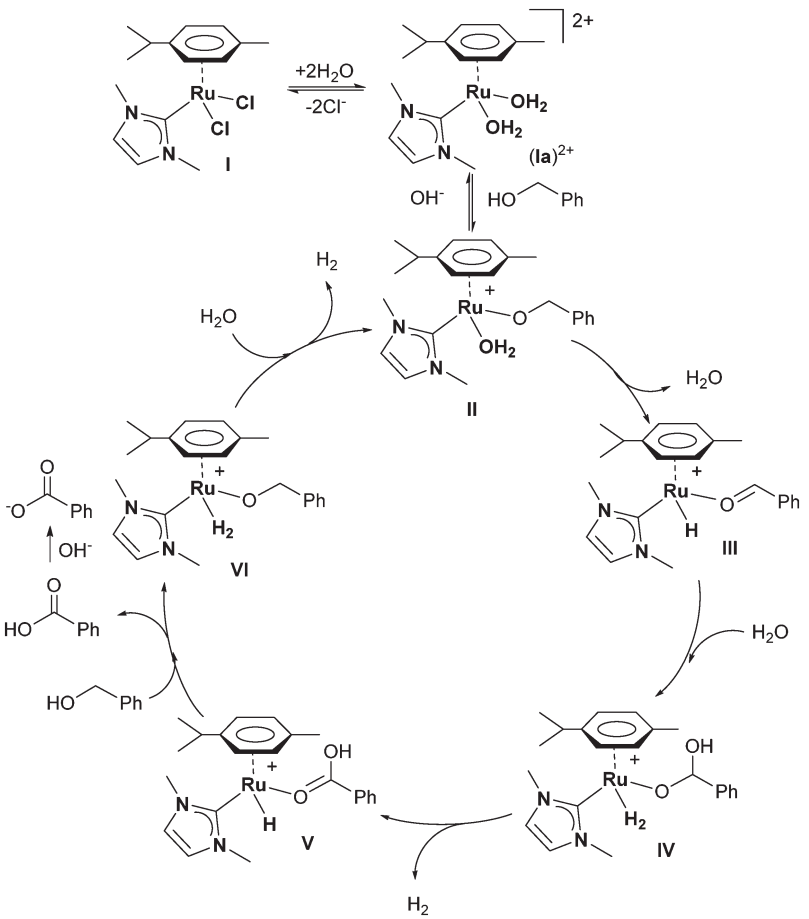

Scheme 2 Proposed mechanism for the synthesis of carboxylic acids from dehydrogenation of primary alcohols.

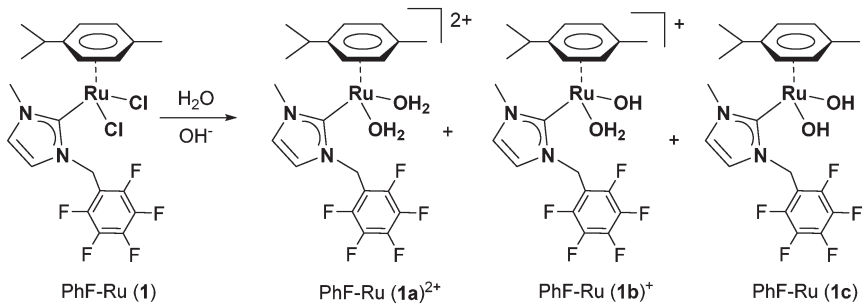

Scheme 3 Aqueous chemical speciation of PhF–Ru (**1**).

catalytic species **II**. The alkoxide complex **II** was characterized by ESI-MS as $[\mathbf{II}\text{-}H_2O]^+$. Subsequent β-hydride elimination generates the ruthenium hydride **III**. This complex **III** was characterized by ESI-MS as $[\mathbf{III}\text{-}PhCHO]^+$. The propensity of this alkoxide species to yield the aldehyde was manifested upon obtaining the collision induced dissociation (CID) spectrum of the species $[\mathbf{II}\text{-}H_2O]^+$ (Fig. S18‡). The CID experiment revealed the exclusive release of aldehyde from the $[\mathbf{II}\text{-}H_2O]^+$ complex concomitant with the formation of a Ru hydride species. Further evidence of aldehyde formation was observed by ^{1}H NMR spectroscopy. In a parallel experiment, the oxidation of *p*-methylbenzyl alcohol was monitored by ^{1}H NMR spectroscopy using D_2O (Fig. 6). *p*-Methylbenzyl alcohol was converted to the corresponding carboxylate within 22 h. During the course of reaction, the dissociation of *p*-methylbenzaldehyde from the ruthenium centre was observed. This is an indication of the formation of species analogous to complex **III** that contains a coordinated aldehyde.

The coordinated aldehyde in **III** undergoes a nucleophilic attack by water, accompanied by protonation of the neighbouring hydride to give the dihydrogen *gem*-diolate **IV**.

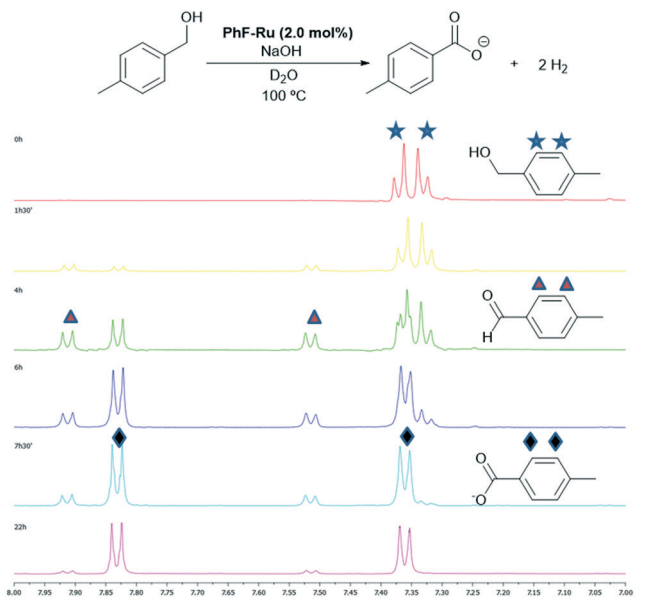

Fig. 6 Monitoring of the reaction by ^{1}H NMR spectroscopy using D_2O.

DFT calculations revealed that molecular hydrogen release and β-hydride elimination are thermodynamically favourable to give complex **V**. Hydride complex **V**, having a coordinated carboxylic acid, reacts with benzyl alcohol to form a molecular hydrogen complex, **VI**, containing dihydrogen and alkoxide ligands. The carboxylic acid is obtained as a carboxylate under basic conditions. Ligand substitution on complex **VI** easily eliminates molecular hydrogen with the regeneration of complex **II**.

DFT calculations were carried out in the gas phase at the M06 level of theory, and solvent corrections were subsequently performed using the SMD solvation model. The theoretical results confirm the proposed mechanism shown in Scheme 2 and agree with the experimental observations obtained by NMR spectroscopy and ESI/MS. The details of the minimized structures, transition states, intermediates, and electronic energies can be found in the ESI.‡ From a thermodynamic point of view, the dehydrogenation of alcohols into carboxylates is an entropically-driven process, boosted by the irreversible release of molecular hydrogen from the reaction media. Experimentally, we have observed that the oxidation of benzyl alcohol does not proceed in a closed vessel, consistent with a reaction in which gas is generated. The release of molecular hydrogen from the reaction media is crucial in the synthesis of carboxylates from alcohols. The formation of hydrogen gas was qualitatively confirmed by gas chromatography.

The complete energy profile is the result of a series of concatenated processes starting from the alkoxide-ruthenium derivative **II** (Fig. 7). The rate-determining step is the nucleophilic attack of water on the coordinated aldehyde complex **III**, which results in the formation of the dihydrogen, *gem*-diolate complex **IV**. The calculated barrier for the overall cycle is 29.8 kcal mol^{-1} ($\mathbf{TS_2}$). As the reaction is carried out in water, the entropic factor is overestimated in the calculation, so the barrier of the real process is expected to be smaller ($\Delta G^{\ddagger}_{\mathbf{III}-\mathbf{IV}}$ = +27.5 kcal mol^{-1}; $\Delta E^{\ddagger}_{\mathbf{III}-\mathbf{IV}}$ = +15.3 kcal mol^{-1}).

DFT calculations show that β-hydrogen elimination is an easy process starting from alkoxides (**II**) or *gem*-diolate ruthenium complexes as shown by the low barrier energy transition states ($\mathbf{TS_1}$ and $\mathbf{TS_3}$). The formation of dihydrogen-alkoxide species **VI** *via* proton transfer from a hydride-alcohol intermediate has an energy barrier of 23.8 kcal mol^{-1} ($\mathbf{TS_4}$).

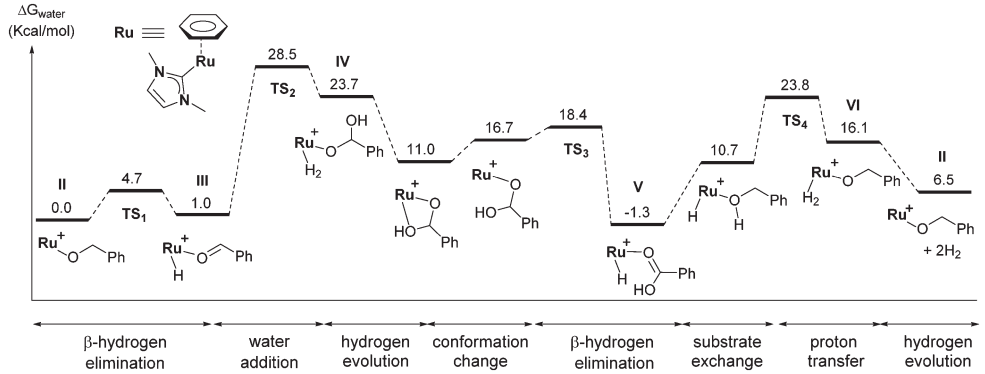

Fig. 7 Relative energy profile for the oxidation of benzyl alcohol to benzoic acid catalysed by [Ru(η^6-C_6H_6)$(Cl)_2$(NHC-Me_2)].

Proton transfer processes are strongly favoured using water as solvent, through the participation of discrete water molecules as proton shuttles. Thus, it is reasonable to argue that the barrier for this process will also be lower than the one calculated through this simulation.

Conclusions

We have developed a straightforward method for the immobilization of ruthenium complexes onto the surface of graphene yielding novel hybrid materials. The ruthenium molecular complexes containing NHC functionalized ligands with different polycyclic aromatic rings were immobilized onto reduced graphene oxide (rGO) by π-stacking interactions. The results show that molecular complexes containing a highly aromatic polycyclic group are easily anchored onto the surface of graphene. The ruthenium complex containing a pyrene fragment is immobilized quantitatively; in contrast, the ruthenium complex containing a pentafluorobenzyl group is barely retained onto the surface of graphene.

The ruthenium complexes and the hybrid materials are active in the catalytic synthesis of carboxylic acids from alcohols in aqueous media. The results showed that the catalytic properties are improved in the hybrid material Pyr–Ru–rGO (**6**) compared to the catalytic outcomes provided by its homogeneous analogue, Pyr–Ru (**3**). The enhanced catalytic properties are a result of the stabilization of the catalytically active species avoiding deactivation pathways. Graphene, as the support, plays a role in the catalytic process through the stabilization of the catalytically active species. The hybrid materials (**4–6**) were reused several times without any significant decrease in activity. The best catalytic results were obtained with the hybrid material containing a pyrene tag, Pyr–Ru–rGO (**6**), which was recycled up to ten times without any decrease in activity. The hybrid materials (**4–6**) show a distinct operating mechanism. Hot filtration experiments revealed that the catalytic properties of the hybrid materials containing a pentafluorobenzyl group PhF–Ru–rGO (**4**) and an anthracenyl group Ant–Ru–rGO (**5**) are governed by a boomerang effect. The molecular ruthenium complexes are anchored and then released from the surface of graphene depending on the temperature. As a result, the catalytic reaction itself is homogeneous in nature. In the case of the hybrid material Pyr–Ru–rGO (**6**), containing a molecular complex with a pyrene tag, no desorption was observed, indicating that the catalysis is heterogeneous and that the molecular complex is strongly anchored to the surface of graphene.

A new mechanism for the catalytic synthesis of carboxylic acids from alcohols has been proposed based on experimental evidence and theoretical calculations. The rate-determining step is the nucleophilic attack of water on the coordinated aldehyde.

This work constitutes a clear step forward in the use of immobilized transition metal complexes as catalysts. The catalytic results offer a practical and easily adaptable methodology that may inspire future developments in efficient heterogeneous catalysis.

Experimental section

General procedures. Graphite powder (natural, universal grade, 200 mesh, 99.9995%) and all other reagents were used as-received from commercial suppliers. Graphene oxide,[60] reduced graphene oxide,[61] $[Ru(p\text{-cym})Cl_2]_2$,[62] complex **3**,[16] and imidazolium salts PhF,[37] Ant,[38] and Pyr[16] were obtained according to known published methods. NMR spectra were recorded on Varian spectrometers operating at 300 or 500 MHz (^{1}H NMR) and 75 and 125 MHz ($^{13}C\{^1H\}$ NMR), respectively, and referenced to $SiMe_4$ (δ in ppm and J in Hertz). Mass spectra were obtained using a QTOF Premier (quadrupole-hexapole-TOF) with an orthogonal Z-spray-electrospray interface (Waters, Manchester, UK).

Synthesis of PhF–Ru (1). Silver oxide (102 mg, 0.44 mmol) was added to a solution of 1-pentafluorobenzyl-3-methylimidazolium bromide (248 mg, 0.72 mmol) in CH_2Cl_2 in a round bottom flask covered with aluminium foil. The suspension was stirred at room temperature for 1 h. Then $[Ru(p\text{-cym})Cl_2]_2$ (200 mg, 0.32 mmol) was added to the suspension and stirred overnight at reflux temperature. After solvent removal, the crude product was purified by column chromatography. Compound **1** was eluted with dichloromethane/acetone (9 : 1). After solvent removal,

compound **1** was obtained as an orange solid. Yield: 120 mg (33%). ^{1}H NMR (500 MHz, $CDCl_3$): δ 6.99 (s, 1H, CH_{imid}), 6.61 (s, 1H, CH_{imid}), 5.65 (s, 2H, NCH_2–), 5.51 (s, 2H, C$H_{p\text{-cym}}$), 5.21 (s, 2H, C$H_{p\text{-cym}}$), 4.00 (s, 3H, NCH_3), 2.96 (m, 1H, C$H_{iPr,p\text{-cym}}$), 2.07 (s, 3H, C$H_{3,p\text{-cym}}$) 1.27 (d, $^3J_{H-H}$ = 6.9 Hz, 6H, C$H_{3,iPr,p\text{-cym}}$). ^{13}C{^{1}H} NMR (125 MHz, $CDCl_3$): δ 175.9 ($C_{carbene}$–Ru), [146.8, 144.8, 142.7, 140.9, 139.0, 136.9] (C–F), [124.5, 120.7] (CH_{imid}), [109.0, 99.1] ($Cq_{p\text{-cym}}$), [85.7, 81.9] ($CH_{p\text{-cym}}$), 44.3 (N–CH_2–), 40.0 (NCH_3), 31.0 ($CH_{iPr,p\text{-cym}}$), 22.3 ($CH_{3,p\text{-cym}}$), 18.8 ($CH_{3,iPr,p\text{-cym}}$). HRMS ESI-TOF-MS (positive mode): [M − Cl]$^+$ monoisotopic peak 533.0357; calc. 533.0359, ε_r 0.4 ppm.

Synthesis of Ant–Ru (2). Silver oxide (102 mg, 0.44 mmol) was added to a solution of 1-(9-methylanthracene)-3-methylimidazolium chloride (223 mg, 0.72 mmol) in CH_2Cl_2 in a round bottom flask covered with aluminium foil. The suspension was stirred at room temperature for 1 h. Then [Ru(*p*-cym)Cl_2]$_2$ (200 mg, 0.32 mmol) was added to the suspension and stirred overnight at reflux temperature. After solvent removal, the crude product was purified by column chromatography. Compound **2** was eluted with dichloromethane/acetone (95 : 5). Recrystallization from a dichloromethane/hexane mixture afforded compound **2** as an orange solid. Yield: 170 mg (46%). ^{1}H NMR (500 MHz, $CDCl_3$): δ 8.52 (s, 1H, CH_{ant}), 8.26 (d, $^3J_{H-H}$ = 8.7 Hz, 2H, CH_{ant}), 8.02 (d, $^3J_{H-H}$ = 8.2 Hz, 2H, CH_{ant}), 7.56–7.40 (m, 4H, CH_{ant}), 6.64 (d, $^3J_{H-H}$ = 2.0 Hz, 1H, CH_{imid}), 6.00 (d, $^3J_{H-H}$ = 1.9 Hz, 1H, CH_{imid}), 5.58 (s, 2H, C$H_{p\text{-cym}}$), 5.36 (s, 2H, C$H_{p\text{-cym}}$), 4.02 (s, 3H, NCH_3), 3.02 (m, 1H, C$H_{iPr,p\text{-cym}}$), 2.24 (s, 3H, C$H_{3,p\text{-cym}}$), 1.31 (d, $^3J_{H-H}$ = 6.9 Hz, 6H, C$H_{3,iPrp\text{-cym}}$). ^{13}C{^{1}H} NMR (125 MHz, C_6D_6): δ 172.6 ($C_{carbene}$–Ru), [131.7, 131.4, 129.3, 129.1, 127.3, 125.4, 125.3, 124.2, 122.7, 121.7] (C_{ant}, CH_{imid}), [108.3, 99.5] ($Cq_{p\text{-cym}}$), [84.8, 82.9] ($CH_{p\text{-cym}}$), 47.7 (N–CH_2–), 39.9 (NCH_3), 31.1 ($CH_{iPr,p\text{-cym}}$), 23.0 ($CH_{3,p\text{-cym}}$), 19.0 ($CH_{3,iPr,p\text{-cym}}$). HRMS ESI-TOF-MS (positive mode): [M − Cl]$^+$ monoisotopic peak 543.1140; calc. 543.1146, ε_r 1.6 ppm.

General procedure for the preparation of M–rGO materials. In a round-bottom flask were introduced 90 mg of rGO and 10 mL of dichloromethane. The suspension was sonicated for 30 minutes. Then, 10 mg of the corresponding metal complex **1–3** was added to the suspension. The mixture was stirred at room temperature for 10 hours. The black solid was filtered off and washed with 2 × 15 mL of dichloromethane. The filtrates were combined and evaporated to dryness under reduced pressure. The presence of unsupported complex **1–3** was analysed by ^{1}H NMR using anisole as the internal standard. Integration of the characteristic signal of anisole (–OMe) *vs.* (NCH_3) accounts for a first indication of the amount of complex deposited onto rGO. The exact amount of supported complex was determined by ICP-MS analysis. Digestion of the materials was performed in a refluxing mixture of nitric and hydrochloric acids (1 : 3) for 12 h.

General procedure for catalytic experiments. Catalytic assays were performed in a round bottom flask, using 0.5 mmol of alcohol, 1 equivalent of cesium carbonate, catalyst and 10 mL of Milli-Q water for 24 hours at 100 °C. Yields and conversions were determined by GC analysis using anisole as the external standard. Isolated yields were determined by ^{1}H NMR using anisole or trimethoxybenzene as the standard.

Recycling experiments were carried out under the same reaction conditions as described in the general procedure. After completion of each run (24 h), the reaction mixture was allowed to reach room temperature and the catalyst was isolated by decantation. The remaining solid was washed thoroughly with water and reused in the following run.

Procedure for hydrogen identification. All glassware was carefully cleaned and rinsed with Milli-Q water prior to use. A 25 mL round bottom flask was charged with 0.44 mmol of 4-methyl benzyl alcohol, 0.44 mmol of cesium carbonate, 8.8 × 10^{-3} mmol of catalyst PhF–Ru (**1**) and 10 mL of water and heated at 100 °C. At selected times, a 1.5 mL sample of the generated gas was collected and the hydrogen content was qualitative analysed by gas chromatography (GS-MOL 15 meters column ID 0.55 mm TCD from J&W Scientific).

X-ray data. Crystallographic details of data collection, structure determination and refinement for complexes PhF–Ru (**1**) and Pyr–Ru (**3**) are summarized in the ESI.‡

Computational details. A full description of theoretical calculations including DFT optimized structures is included in the ESI.‡

Associated content

Experimental procedures, characterization of new molecular complexes and hybrid materials, crystallographic data, computational details and analysis.

Author contributions

D. V.-E. prepared the complexes and performed the catalytic experiments. C. V. conducted mechanistic studies by ESI/MS. M. B. performed mechanistic studies by DFT calculations. All the authors discussed the final version of the article.

Acknowledgements

The authors acknowledge the financial support from MINECO (CTQ2015-69153-C2-2-R and CTQ2015-67461-P), Generalitat Valenciana (AICO/2015/039), Universitat Jaume I (P1.1B2015-09) and Universidad de Zaragoza (UZ2014-CIE-01). The authors are very grateful to the 'Serveis Centrals d'Instrumentació Científica (SCIC)' of the Universitat Jaume I, Instituto de Biocomputación y Física de Sistemas Complejos (BIFI) and the Centro de Supercomputación de Galicia (CESGA) for generous allocation of computational resources.

Notes and references

1 *Recoverable and Recyclable Catalysts*, ed. M. Benaglia, John Wiley & Sons, Ltd, Chichester, UK, 2009.
2 R. H. Crabtree, *Chem. Rev.*, 2012, **112**, 1536–1554.

3 D. Astruc, F. Lu and J. R. Aranzaes, *Angew. Chem., Int. Ed.*, 2005, **44**, 7852–7872.
4 M. P. Conley, C. Copéret and C. Thieuleux, *ACS Catal.*, 2014, **4**, 1458–1469.
5 T. K. Maishal, J. Alauzun, J.-M. Basset, C. Copéret, R. J. P. Corriu, E. Jeanneau, A. Mehdi, C. Reyé, L. Veyre and C. Thieuleux, *Angew. Chem., Int. Ed.*, 2008, **47**, 8654–8656.
6 A. Corma and H. Garcia, *Adv. Synth. Catal.*, 2006, **348**, 1391–1412.
7 J. A. Gladysz, *Pure Appl. Chem.*, 2001, **73**, 1319–1324.
8 P. Serna and B. C. Gates, *Acc. Chem. Res.*, 2014, **47**, 2612–2620.
9 C. Huang, C. Li and G. Shi, *Energy Environ. Sci.*, 2012, **5**, 8848.
10 S. Navalon, A. Dhakshinamoorthy, M. Alvaro and H. Garcia, *Chem. Rev.*, 2014, **114**, 6179–6212.
11 B. F. Machado and P. Serp, *Catal. Sci. Technol.*, 2012, **2**, 54–75.
12 M. Blanco, P. Álvarez, C. Blanco, M. V. Jiménez, J. Fernández-Tornos, J. J. Pérez-Torrente, J. Blasco, G. Subías, V. Cuartero, L. A. Oro and R. Menéndez, *Carbon*, 2016, **96**, 66–74.
13 V. Georgakilas, M. Otyepka, A. B. Bourlinos, V. Chandra, N. Kim, K. C. Kemp, P. Hobza, R. Zboril and K. S. Kim, *Chem. Rev.*, 2012, **112**, 6156–6214.
14 J. A. Mann and W. R. Dichtel, *ACS Nano*, 2013, **7**, 7193–7199.
15 J. A. Mann and W. R. Dichtel, *J. Phys. Chem. Lett.*, 2013, **4**, 2649–2657.
16 S. Sabater, J. A. Mata and E. Peris, *ACS Catal.*, 2014, **4**, 2038–2047.
17 S. Sabater, J. A. Mata and E. Peris, *Organometallics*, 2015, **34**, 1186–1190.
18 S. Ruiz-Botella and E. Peris, *Chem. – Eur. J.*, 2015, **21**, 15263–15271.
19 S. Hübner, J. G. de Vries and V. Farina, *Adv. Synth. Catal.*, 2016, **358**, 3–25.
20 J. G. de Vries, *Top. Catal.*, 2014, **57**, 1306–1317.
21 R. A. Sheldon, I. W. C. E. Arends and A. Dijksman, *Catal. Today*, 2000, **57**, 157–166.
22 R. A. Sheldon, *Metal-Catalyzed Reactions in Water*, Wiley-VCH Verlag GmbH & Co. KGaA, Weinheim, Germany, 2013.
23 C. Gunanathan and D. Milstein, *Science*, 2013, **341**, 1229712.
24 M. Trincado, D. Banerjee and H. Grützmacher, *Energy Environ. Sci.*, 2014, **7**, 2464.
25 D. Spasyuk, S. Smith and D. G. Gusev, *Angew. Chem., Int. Ed.*, 2012, **51**, 2772–2775.
26 R. A. Sheldon, *Chem. Soc. Rev.*, 2012, **41**, 1437–1451.
27 E. Balaraman, E. Khaskin, G. Leitus and D. Milstein, *Nat. Chem.*, 2013, **5**, 122–125.
28 J. Malineni, H. Keul and M. Möller, *Dalton Trans.*, 2015, **44**, 17409–17414.
29 A.-K. C. Schmidt and C. B. W. Stark, *Org. Lett.*, 2011, **13**, 4164–4167.
30 J.-H. Choi, L. E. Heim, M. Ahrens and M. H. G. Prechtl, *Dalton Trans.*, 2014, **43**, 17248–17254.
31 G. J. Ten Brink, I. W. C. E. Arends and R. A. Sheldon, *Science*, 2000, **287**, 1636–1639.
32 T. Zweifel, J. V. Naubron and H. Grützmacher, *Angew. Chem., Int. Ed.*, 2009, **48**, 559–563.
33 E. Alberico and M. Nielsen, *Chem. Commun.*, 2015, **51**, 6714–6725.
34 P. Hu, Y. Diskin-Posner, Y. Ben-David and D. Milstein, *ACS Catal.*, 2014, **4**, 2649–2652.
35 M. Nielsen, E. Alberico, W. Baumann, H.-J. Drexler, H. Junge, S. Gladiali and M. Beller, *Nature*, 2013, **495**, 85–89.
36 R. E. Rodríguez-Lugo, M. Trincado, M. Vogt, F. Tewes, G. Santiso-Quinones and H. Grützmacher, *Nat. Chem.*, 2013, **5**, 342–347.
37 S. McGrandle and G. C. Saunders, *J. Fluorine Chem.*, 2005, **126**, 449–453.
38 G. M. Blackburn, G. Lockwood and V. Solan, *J. Chem. Soc., Perkin Trans. 2*, 1976, 1452–1456.
39 S. M. Jackson, D. M. Chisholm, J. S. McIndoe and L. Rosenberg, *Eur. J. Inorg. Chem.*, 2011, 327–330.
40 L. S. Santos, G. B. Rosso, R. A. Pilli and M. N. Eberlin, *J. Org. Chem.*, 2007, **72**, 5809–5812.
41 C. Janiak, *J. Chem. Soc., Dalton Trans.*, 2000, 3885–3896.
42 A. Hirsch, J. M. Englert and F. Hauke, *Acc. Chem. Res.*, 2013, **46**, 87–96.
43 Y. Sun, S. Yang, G. Zhao, Q. Wang and X. Wang, *Chem. – Asian J.*, 2013, **8**, 2755–2761.
44 D. R. Dreyer, H. P. Jia and C. W. Bielawski, *Angew. Chem., Int. Ed.*, 2010, **49**, 6813–6816.
45 H.-P. Jia, D. R. Dreyer and C. W. Bielawski, *Tetrahedron*, 2011, **67**, 4431–4434.
46 D. R. Dreyer, A. D. Todd and C. W. Bielawski, *Chem. Soc. Rev.*, 2014, **43**, 5288–5301.
47 J. C. Espinosa, S. Navalón, A. Primo, M. Moral, J. F. Sanz, M. Álvaro and H. García, *Chem. – Eur. J.*, 2015, **21**, 11966–11971.
48 G. Liu, B. Wu, J. Zhang, X. Wang, M. Shao and J. Wang, *Inorg. Chem.*, 2009, **48**, 2383–2390.
49 F. Li, B. Zhang, X. Li, Y. Jiang, L. Chen, Y. Li and L. Sun, *Angew. Chem., Int. Ed.*, 2011, **50**, 12276–12279.
50 P. D. Tran, A. Le Goff, J. Heidkamp, B. Jousselme, N. Guillet, S. Palacin, H. Dau, M. Fontecave and V. Artero, *Angew. Chem., Int. Ed.*, 2011, **50**, 1371–1374.
51 J. Wei, X. Zhang, X. Zhang, Y. Zhao, R. Li and Q. Yang, *ChemCatChem*, 2014, **6**, 1368–1374.
52 C. Vriamont, M. Devillers, O. Riant and S. Hermans, *Chem. – Eur. J.*, 2013, **19**, 12009–12017.
53 R. H. Crabtree, *Chem. Rev.*, 2015, **115**, 127–150.
54 J. E. Hamlin, K. Hirai, V. C. Gibson and P. M. Maitlis, *J. Mol. Catal.*, 1982, **15**, 337–347.
55 K. Yu, W. Sommer, M. Weck and C. W. Jones, *J. Catal.*, 2004, **226**, 101–110.
56 D. A. Conlon, B. Pipik, S. Ferdinand, C. R. LeBlond, J. R. Sowa, B. Izzo, P. Collins, G. J. Ho, J. M. Williams, Y. J. Shi and Y. Sun, *Adv. Synth. Catal.*, 2003, **345**, 931–935.
57 A. Biffis, M. Zecca and M. Basato, *Eur. J. Inorg. Chem.*, 2001, 1131–1133.

58 P. Csabai and F. Joó, *Organometallics*, 2004, **23**, 5640–5643.
59 J. Díez, J. Gimeno, A. Lledós, F. J. Suárez and C. Vicent, *ACS Catal.*, 2012, **2**, 2087–2099.
60 W. S. Hummers and R. E. Offeman, *J. Am. Chem. Soc.*, 1958, **80**, 1339.
61 S. Stankovich, D. A. Dikin, R. D. Piner, K. A. Kohlhaas, A. Kleinhammes, Y. Jia, Y. Wu, S. T. Nguyen and R. S. Ruoff, *Carbon*, 2007, **45**, 1558–1565.
62 M. A. Bennett and A. K. Smith, *J. Chem. Soc., Dalton Trans.*, 1974, 233.